ADVANCED MATERIALS
www.advmat.de

A Biomimetic Autophagosomes-Based Nanovaccine Boosts Anticancer Immunity

Liping Qu, Guanhong Cui, Yinping Sun, Ruonan Ye, Yu Sun, Fenghua Meng, Shenqiang Wang, and Zhiyuan Zhong**

Personalized cancer vaccines based on tumor cell lysates offer promise for cancer immunotherapy yet fail to elicit a robust therapeutic effect due to the weak immunogenicity of tumor antigens. Autophagosomes, obtained from pleural effusions and ascites of cancer patients, have been identified as abundant reservoirs of tumor neoantigens that exhibit heightened immunogenicity. However, their potential as personalized cancer vaccines have been constrained by suboptimal lymphatic-targeting performances and challenges in antigen-presenting cell endocytosis. Here,a reinforced biomimetic autophagosome-based (BAPs) nanovaccine generated by precisely amalgamating autophagosome-derived neoantigens and two types of adjuvants capable of targeting lymph nodes is developed to potently elicit antitumor immunity. The redox-responsive BAPs facilitate cytosolic vaccine opening within antigen-presenting cells, thereby exposing adjuvants and antigens to stimulate a strong immune response. BAPs evoke broad-spectrum T-cell responses, culminating in the effective eradication of 71.4% of established tumors. Notably, BAPs vaccination triggers enduring T-cell responses that confer robust protection, with 100% of mice shielded against tumor rechallenge and a significant reduction in tumor incidence by 87.5%. Furthermore, BAPs synergize with checkpoint blockade therapy to inhibit tumor growth in the poorly immunogenic breast cancer model. The biomimetic approach presents a powerful nanovaccine formula with high versatility for personalized cancer immunotherapy.

1. Introduction

Personalized cancer vaccines represent a groundbreaking approach to cancer treatment, aiming to provoke and enhance both innate and adaptive immune responses against tumor antigen (Ag), ultimately targeting and eliminating tumor cells.[1] Recent advancements in personalized vaccination strategies have emphasized the co-delivery of selected tumor-specific Ag and immunoadjuvants to antigen-presenting cells (APCs), particularly dendritic cells (DCs), to trigger tumor-specific immune reactions.[2] Considerable research has been devoted to leveraging self-antigens aberrantly expressed in tumors, known as tumor-associated antigens (TAAs), for customizing vaccines.[3] However, attempts using tumor cell-derived components like cell lysates, cell-derived nanovesicles, or extracted cell membranes as TAAs have encountered challenges in generating clinically potent antitumor immune responses, largely due to the limited immunogenicity of these Ag.[4] Moreover, autologous tumor cell-derived vaccines necessitate tumor resection, which not only restricts access to tumor Ag in cases of unresectable tumors but also heightens the risk of metastasis.[5] Therefore, the imperative lies in the development of personalized cancer vaccines with high specificity and immunogenicity, obviating the necessity for tumor excision.

Autophagy, a tightly regulated and stress-induced catabolic pathway in all eukaryotes, has been reported to play essential roles in antigen presentation and eliciting host cell immunity.[6] Autophagosomes, which are enriched by modulation of bulk degradation pathways, comprise a broader repertoire of tumor-specific Ag, giving rise to the generation of Ag peptide presented by the major histocompatibility complex class I (MHC-I) on tumor cells.[7] Previous research demonstrated that tumor cell-derived autophagosomes (TRAPs) vaccines, which are enriched with autophagosome-packaged cellular proteins, defective ribosomal products (DRiPs), short-lived proteins (SLiPs), and surface markers, have demonstrated greater efficacy in mediating tumor regression compared to vaccines derived from whole tumor cells, as evidenced by experimental and clinical studies.[8] Notably, clinical trials demonstrated that TRAPs could be directly isolated from malignant pleural effusions and ascitic fluid.[9] Despite boosted immunizations induced by TRAPs, limitations exist, such as the suboptimal size of

L. Qu, G. Cui, Y. Sun, R. Ye, Y. Sun, F. Meng, Z. Zhong
Biomedical Polymers Laboratory
College of Chemistry
Chemical Engineering and Materials Science
and State Key Laboratory of Radiation Medicine and Protection
Soochow University
Suzhou 215123, P. R. China
E-mail: zyzhong@suda.edu.cn
S. Wang, Z. Zhong
College of Pharmaceutical Sciences
Soochow University
Suzhou 215123, P. R. China
E-mail: wangshenqiang@suda.edu.cn
The ORCID identification number(s) for the author(s) of this article can be found under https://doi.org/10.1002/adma.202409590

DOI: 10.1002/adma.202409590

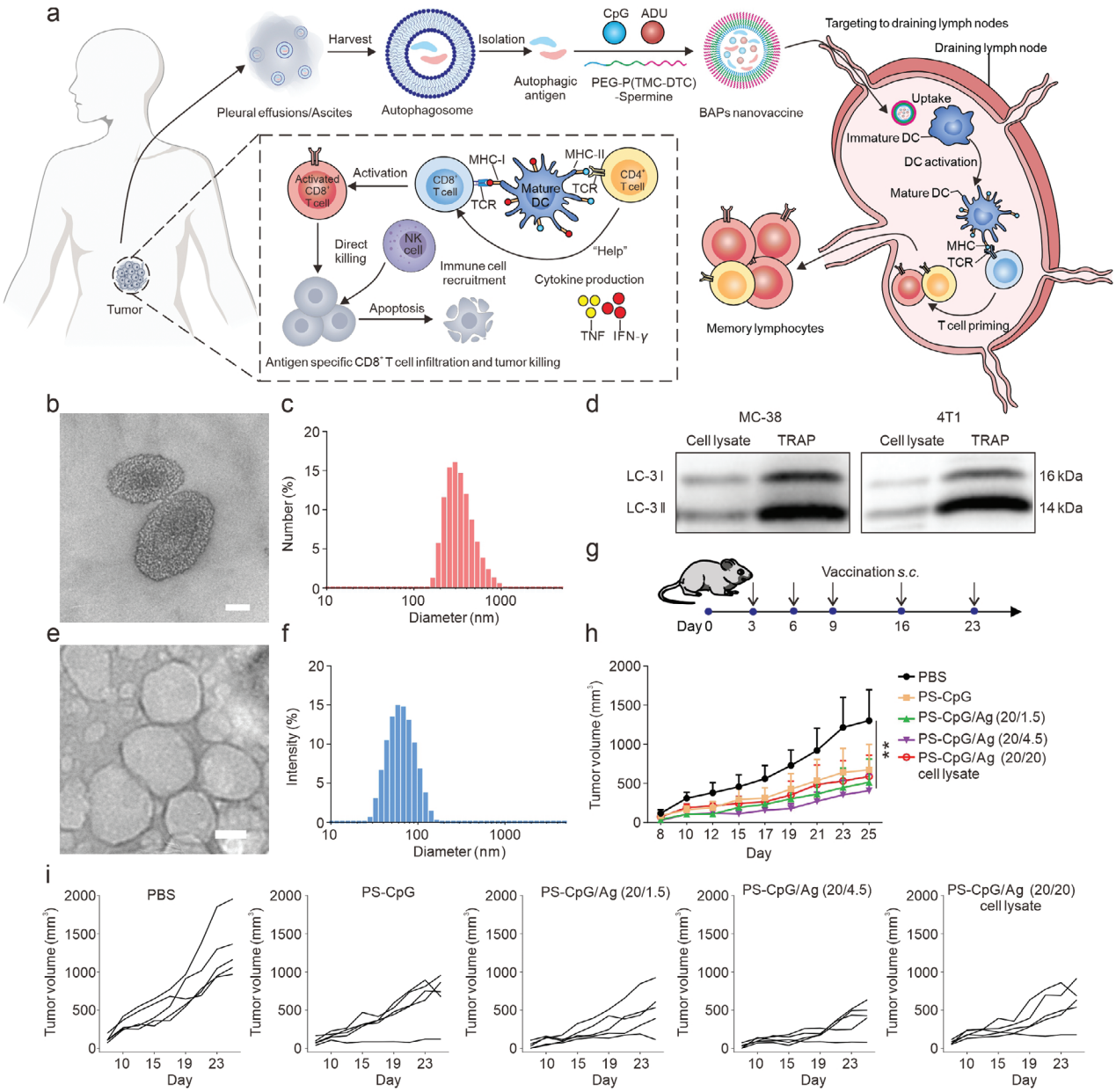

Figure 1. Design and immunization of biomimetic autophagosome-based (BAPs) nanovaccines. a) Schematic illustration of the construction of BAPs and the utilization of BAPs for efficient cancer immunotherapy. Autophagosomes could be isolated from pleural effusions or ascites of patients. By encapsulating autophagic proteins and adjuvants within self-assembled nanovesicles, BAPs are formulated to efficiently transport Ag and adjuvants to draining lymph nodes (dLNs). Such an approach triggers DCs maturation and facilitates antigen presentation, ultimately inducing a robust, antigen-specific immune response for effective cancer immunotherapy. b) TEM image of autophagosomes. Scale bar: 100 nm. c) The size distribution histogram of autophagosomes. d) Western blot (WB) evaluation of autophagic marker LC-3I and LC-3II in both cell lysates and TRAPs from MC38 cells and 4T1 cells. e) TEM image of BAPs. Scale bar: 10 nm. f) The size distribution histogram of BAPs. g) Experimental outline showing the treatment steps. h) Average tumor growth curves of MC38-bearing mice after various treatments indicated ($n = 5$ biologically independent samples). i) Individual tumor growth curves of mice after different treatments. Data are presented as mean ± SD and statistical significance was analyzed via one-way ANOVA with Tukey's multiple comparison test. p value: $^{**}p < 0.01$.

TRAPs for endocytosis and its poor targeting of lymph nodes (LNs).[10] Consequently, the effective delivery of Ag and adjuvants to the LNs, where dendritic cell (DC) maturation occurs and antigen cross-presentation stimulates a controlled yet robust tumor-specific T-cell response, stands out as a critical challenge.[11]

Here, we present a biomimetic autophagosomes (BAPs)-based approach to provoke a robust tumor-specific immune response for personalized cancer immunotherapy (**Figure 1a**). Reinforced BAPs are fabricated by incorporating neoantigens sourced from TRAPs and adjuvants into self-assembled nanovesicles. Precise modulation of the nanovaccine components allows for

accurate dosage control. Additionally, the engineered BAPs shield the cargo from extracellular proteases, facilitating effective transportation to draining lymph nodes (dLNs). Through endocytosis by DCs, the neoantigen and adjuvants are responsively released at specific subcellular functional sites, leading to significantly elevated DCs maturation and boosted cross-reactive T-cell responses. Potent antigen-specific $CD8^+$ cytotoxic T lymphocytes (CTLs) responses, as well as efficient immune-mediated tumor regression and prevention of tumor recurrence, are demonstrated in colorectal cancer models in vivo. Such BAPs-based nanovaccines, when combined with immune checkpoint blockade (ICB), can suppress the growth of poorly immunogenic tumors. To our knowledge, this study represents the first application of autophagosome-derived nanovaccines in the realm of cancer immunotherapy. The BAPs nanovaccine provides an efficient and clinically translational strategy to boost intense immune responses for personalized cancer immunotherapy.

2. Results and Discussions

2.1. Biomimetic Autophagosomes (BAPs) for Antigen and Adjuvant Delivery

To demonstrate the proof-of-concept, autophagosomes were isolated from cancer cells. To safeguard Ag within the autophagosomes, autophagy was first stimulated in the cancer cells, followed by the inhibition of lysosome or proteasome activity (Figure S1a, Supporting Information).[12] Nutrient deprivation and hypoxic stress contributed to the elevated induction of autophagy, and antigens derived from autophagosomes facilitated tumor growth inhibition (Figures S1b–d, Supporting Information). Subsequently, the supernatant of treated cells was centrifuged to obtain autophagosomes, as evidenced by the transmission electron microscopy (TEM) imaging and the autophagosome marker lapidated microtubule-associated protein 1A/1B-light chain 3 (LC3) (Figure 1b–d). Through ultrasonication, antigen-enriched autophagic proteins were collected. BAPs, with an average diameter of 61 nm, were fabricated by self-assembly of Ag and adjuvants within poly(ethylene glycol)-*b*-poly(trimethylene carbonate-*co*-dithiolane trimethylene carbonate)-spermine (PEG-P(TMC-DTC)-SP) (PS) nanovesicles (Figure 1e,f, Figure S2, Supporting Information). BAPs, featuring pendant dithiolane groups, facilitate the direct transportation of Ag and adjuvants into the reductive cytosol of APCs. The drug loading efficiencies of Ag, Toll-like receptors-9 (TLR-9) agonist CpG oligonucleotide, and stimulator of interferon genes (STING) agonist ADU in BAPs were 85%, 90%, and 50%, respectively (Table S1, Supporting Information).

We then investigated the impact of Ag content on tumor regression. BAPs formulated with varied amounts of Ag were subcutaneously injected at the tail base of MC-38 colon carcinoma-bearing C57BL/6 mice (Figure 1g).[13] While PS nanovesicles loaded with CpG (20 μg per mouse) inhibited tumor growth to some extent, the addition of Ag dramatically amplified the inhibitory effect. Mice injected with BAPs-4.5 (BAPs loaded with 4.5 μg Ag per mouse) demonstrated notably smaller average tumor volumes compared to other groups at all time points (Figure 1h,i). We further compared the immunogenicity of Ag derived from TRAPs and tumor cell lysates. Notably, our BAPs nanovaccine, which contained a lower quantity of antigens, demonstrated significantly greater tumor growth inhibition than the nanovaccine formulated with tumor cell lysis-derived antigens, which contained 4.4 times more antigens. This finding indicates that antigens derived from autophagosomes exhibit higher immunogenicity. Minimal fluctuations in body weights were observed, indicating satisfactory biocompatibility (Figure S3, Supporting Information).

2.2. BAPs Promote the Endocytosis and Activation of DCs

The interactions between BAPs and DCs were comprehensively investigated. More BAPs have been endocytosed by DC2.4 compared to TRAPs, as evidenced by the stronger cytosolic fluorescent signals of Ag (**Figure 2**a; Figures S4a–c, Supporting Information). Moreover, the disulfide-crosslinked BAPs nanovaccine resulted in redox-triggered decrosslinking within DCs, thereby exposing adjuvants and antigens to evoke an immune response.[14] The maturation of DCs, critical for antigen presentation and the initiation of subsequent immune responses, was further examined. Flow cytometry analysis revealed that bone marrow-derived dendritic cells (BMDCs) pulsed with PS nanovesicles loaded with Ag and CpG revealed increased upregulation in co-stimulatory molecules (CD86, and MHC-II) (Figure 2b,c). Additionally, the introduction of ADU further promoted BMDCs activation when compared to the other groups. Therefore, we used CpG and ADU as adjuvants in the subsequent experiments. Secretion of pro-inflammatory cytokines, including interleukin-6 (IL-6), IL-12p70, IL-1β, tumor necrosis factor-α (TNF-α), and interferon-β (IFN-β), from BMDCs treated with BAPs was markedly elevated, in contrast to the limited effects observed in the control groups (Figure 2d).

To investigate the lymphatic delivery of Ag and adjuvants in vivo, fluorophore-tagged TRAPs or Ag were subcutaneously injected at the tail base of C57BL/6 mice. The inguinal LNs and major organs were harvested 24 h post-injection for *ex vivo* imaging (Figure 2e,f, Figure S5, Supporting Information). BAPs elicited the highest fluorescence signals in the LNs, compared to TRAPs, Ag, and dyes, thus verifying that our biomimetic approach promotes in vivo delivery of nanovaccines to LNs (Figure 2g,h). Subsequently, we immunized C57BL/6 mice with BAPs or control formulations at equivalent doses of Ag and adjuvants, followed by the analysis of the draining LNs 1-day post-injection (Figure 2i). In contrast with the Ag group and the physical mixture group, the elevated proportion of matured DCs ($CD80^+CD86^+CD11c^+$) (Figure 2j) and activated DCs ($CD11c^+$MHC-II^+) (Figure 2k) within the dLNs of mice treated with BAPs was observed. Moreover, BAPs immunization also contributed to intensive humoral immunity, as indicated by the incremental percentage of B cells (Figure S6a, Supporting Information). The incorporation of ADU also led to the activation of NKG2D positive natural killer (NK) cells (Figure S6b, Supporting Information).[15] Altogether, BAPs were proved to be more effective in directed trafficking to secondary lymphoid organs, inducing antigen cross-presentation, and eliciting robust immune responses.

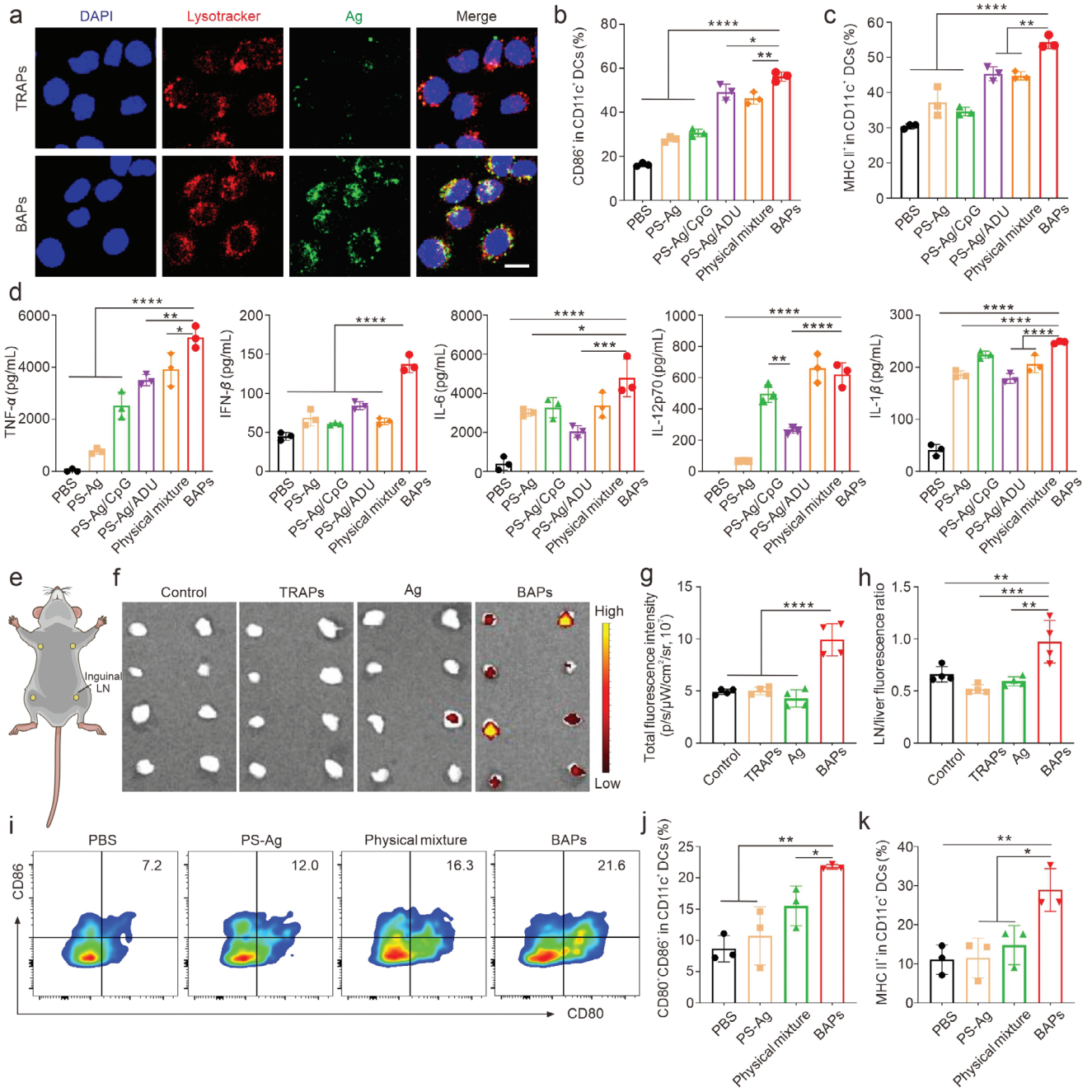

Figure 2. Targeted delivery of Ag and adjuvants into dLNs and the induction of robust uptake and DC maturation. a) Confocal microscopy images showing Ag subcellular localization in DC2.4 after incubating for 6 h. Scale bar: 10 μm. b) The percentage of activated BMDCs quantified by flow cytometric analysis of BMDCs incubated with the indicated formulations ($n = 3$ biologically independent samples). c) Flow cytometry analysis of MHC-II expression on murine BMDCs ($n = 3$ biologically independent samples). d) The canonical proinflammatory cytokines secreted from BMDCs exposed to the indicated formulations ($n = 3$ biologically independent samples). e) Scheme of the localization of inguinal dLNs. f) *Ex vivo* fluorescent images of inguinal dLNs. Cy5-tagged Ag or the Cy5-labelled TRAPs and BAPs were subcutaneously injected into mice ($n = 4$ biologically independent samples) at the tail base. g) Quantification of the total fluorescence intensity of dLNs in f. h) Quantification of the fluorescence intensity ratio of dLN/liver ($n = 4$ biologically independent samples). i–k) Representative flow cytometry plots (i) and quantifications of $CD80^+CD86^+$ (j) and MHC-II^+ (k) DCs, indicating DC maturation induced by different formulations in vivo on day 1 post-immunization ($n = 3$ biologically independent samples). Data are presented as mean ± SD and statistical significance was analyzed via one-way ANOVA with Tukey's multiple comparison test. p value: $^{*}p < 0.05$, $^{**}p < 0.01$, $^{***}p < 0.001$, $^{****}p < 0.0001$.

2.3. BAPs-Based Personalized Nanovaccine Inhibits Tumor Growth In Vivo

The therapeutic performance of BAPs was evaluated using the MC-38 colon carcinoma model, employing PBS as well as PS nanovesicles loaded with Ag (PS-Ag) or adjuvant (PS-Ag/CpG and PS-Ag/ADU), alongside a physical mixture of Ag and adjuvants (physical mixture) as control groups. MC-38 is a murine colorectal cancer cell line distinguished by clinically significant mutations and a pronounced level of aggressiveness.[16] Consequently, vaccination was commenced on day 3 following tumor implantation, as previously documented (**Figure 3**a).[17] Mice treated with PBS experienced 100% mortality within 30 days (Figure 3b). Meanwhile, the PS-Ag, PS-Ag/CpG, and PS-Ag/ADU treatment groups demonstrated suboptimal immune therapeutic responses. The physical mixture group showed a modest degree (42.9%) of tumor inhibition (Figure 3c). In contrast, treatment with BAPs led to accelerated tumor regression, with ≈71.4% of treated mice achieving complete regression lasting over 60 days, exhibiting superior therapeutic efficacy relative to earlier investigations (Figure 3d).[17a,18] No discernible signs of organ damage or inflammatory lesions were detected in mice receiving BAPs (Figure S7, Supporting Information). Inconspicuous fluctuations in body weights were also verified (Figure S8, Supporting Information).

The investigation of T-lymphocyte infiltration in tumor tissues harvested from mice immunized with either BAPs or control formulations was conducted. The control groups resulted in minimal T-cell responses, whereas an evident elevated proportion of $CD8^+$ tumor-infiltrating T lymphocytes (TILs) in the BAPs-treated mice was observed (Figure 3e,f, Figure S9, Supporting Information). Moreover, the mice immunized with BAPs also revealed a higher ratio of IFN-γ^+CD8^+ T cells (Figure 3g,h) and $CD107a^+CD8^+$ T cells (Figure S10, Supporting Information) within the spleen, indicating the activation of systemic CTLs. Furthermore, the BAPs promoted the recruitment of $CD4^+$ helper T cells (Figure 3i,j), while suppressing $CD4^+CD25^+FoxP3^+$ regulatory T cells (Figure 3k, Figure S11, Supporting Information), implying the critical role of $CD4^+$ T cells in tumor regression. Evaluation of memory T cells in peripheral blood mononuclear cells (PBMCs) obtained from mice subjected to different treatments revealed significantly increased proportions of effector memory $CD8^+CD44^+CD62L^-$T cells (Figure 3l) and $CD4^+CD44^+CD62L^-$ T cells (Figure 3m) following BAPs vaccination. The marked IFN-γ^+ ELISPOT (enzyme-linked immune absorbent spot) responses in the splenocytes (Figure 3n,o), along with the incremental IFN-γ (Figure 3p) and TNF-α (Figure 3q) cytokine secretion in the serum, were observed in the BAPs group compared with the control groups. These results reveal the potential of our biomimetic strategy in eliciting robust anti-tumor immune responses and establishing enduring immune memory.

2.4. BAPs Vaccination Protects Against Tumor Rechallenge and Prevents Tumor Occurrence

We further investigated whether the BAPs could provide durable protection extending beyond 100 days in an MC-38 tumor rechallenge model. Following inoculation of MC-38 colon adenocarcinoma cells in surviving mice from the BAPs-vaccinated group, all rechallenged mice exhibited complete tumor eradication, achieving a tumor inhibition rate of 100% (**Figure 4**a–c). This outcome underscores that BAPs induced robust immunological memory to prevent tumor recurrence. Subsequently, memory T cells in PBMCs, spleen, and LNs were subjected to flow cytometry analysis. Both effector memory $CD4^+$ and $CD8^+$ ($CD4^+CD44^+CD62L^-$ and $CD8^+CD44^+CD62L^-$) T cells were elevated in these organs as a result of BAPs vaccination (Figure 4d–f).

The prophylactic efficacy of BAPs was further evaluated. Mice were initially subcutaneously immunized with BAPs at the tail base four times (Figure 4g). One week after the last immunization, MC-38 colon adenocarcinoma cells were subcutaneously inoculated. Remarkably, vaccination with BAPs significantly prevented the formation of tumors, leading to complete tumor rejection, with 87.5% of mice surviving beyond 60 days without noticeable changes in body weight (Figure 4h–j, Figure S12, Supporting Information). The phenotype of T cells was further elucidated. PBMCs obtained from BAPs-immunized mice exhibited elevated frequencies of $CD8^+$ T cells and effector memory T cells compared to the control group (Figure 4k–m). Additionally, BAPs also stimulated higher secretion of pro-inflammatory cytokines, including TNF-α, IFN-γ, and IL12p70 (Figure 4n). These results suggest that BAPs offer not only specific long-acting protection but also robust immunity against tumor occurrence.

2.5. Tumor Eradication by Combination Immunotherapy with BAPs and Immune Checkpoint Blockade

Encouraged by the substantial anticancer efficacy of BAPs in tumor eradication and prevention observed in the MC-38 colon carcinoma model, we further explored their potential effectiveness in a highly aggressive and poorly immunogenic tumor model.[19] Consequently, the 4T1 breast cancer model was employed to assess the therapeutic efficacy of BAPs on "cold" tumors. We also investigated whether the co-administration of a clinically approved immune checkpoint inhibitor, anti-cytotoxic T-lymphocyte-associated protein 4 antibody (anti-CTLA4), could enhance the effectiveness of BAPs (**Figure 5**a).[20] Vaccination with BAPs resulted in delayed tumor growth, with 2 out of 6 mice achieving tumor regression and becoming tumor-free (Figure 5b–d). Although anti-CTLA4 treatment alone appeared to be less effective, the combination of BAPs and anti-CTLA4 exhibited impressive therapeutic effects in inhibiting tumors, leading to a 50% increase in survival rate over 90 days. Given the essential role of $CD4^+$ and $CD8^+$ T cells in adaptive immune responses, we evaluated T-cell infiltrates in the spleen of mice. Treatment with anti-CTLA4 alone minimally impacted T cell populations, whereas the combination therapy showed higher fractions of $CD8^+CD3^+$ effector and $CD4^+CD3^+$ helper T cells within the splenocytes (Figure 5e–g). Similarly, the proportion of cytotoxic T cells (IFN-γ^+CD8^+ and IFN-γ^+CD4^+ T cells) was also elevated in the combination group (Figure 5h–j). In addition, the combinatorial treatment could also effectively reverse the enlargement of spleens in 4T1 tumor-bearing mice back to baseline levels, indicating a reduction in systemic inflammation to a normal range, which is crucial for ensuring the safe administration of BAPs (Figure 5k,l). An increase in $CD69^+CD8^+$

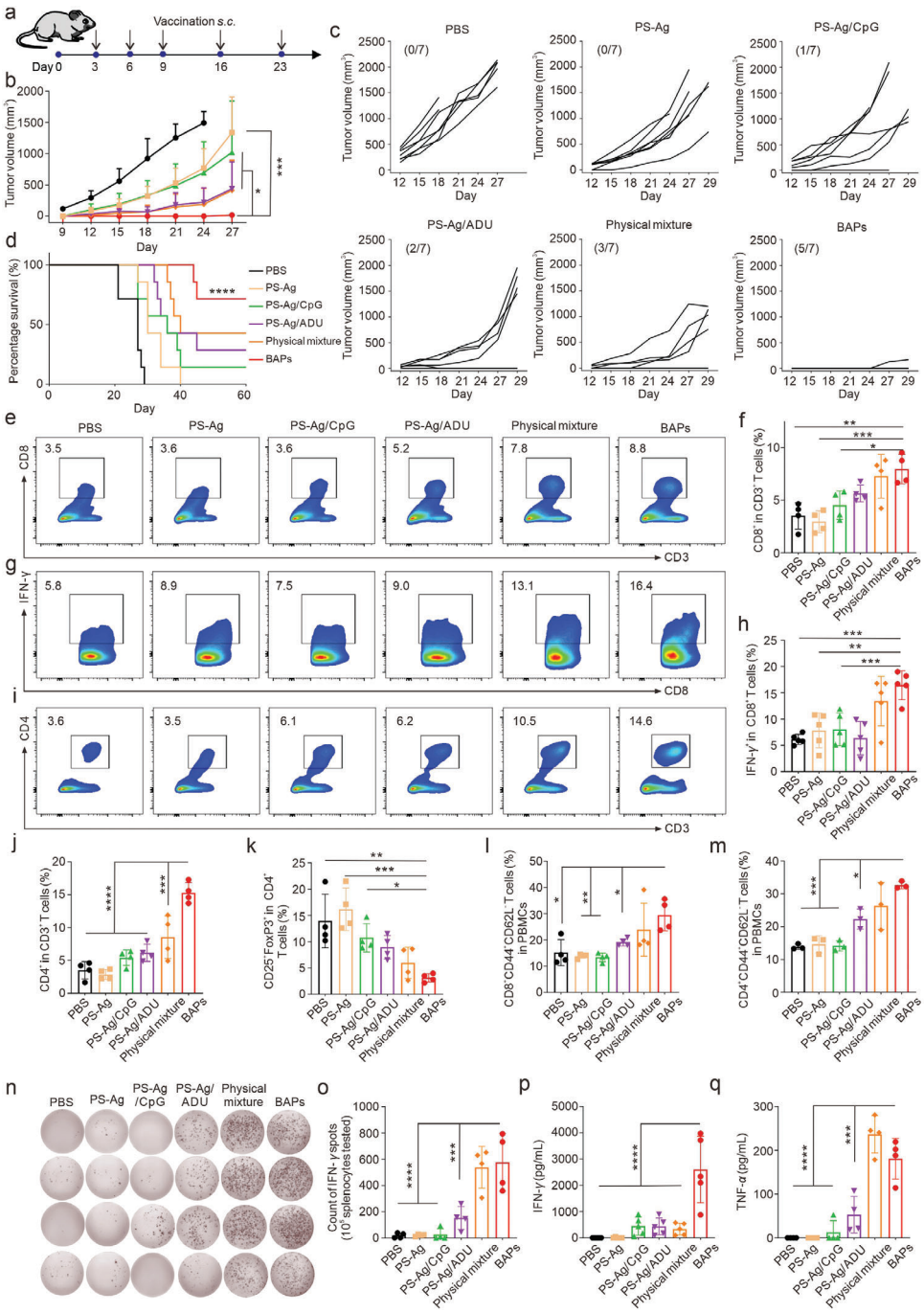

Figure 3. The BAPs efficiently inhibit tumor growth and improve the survival of tumor-bearing mice. a) The timeline of the experimental design to evaluate the in vivo therapeutic performance of BAPs. b) Average tumor growth curves of MC-38-bearing mice after various treatments indicated ($n = 7$ biologically independent samples). c) Individual tumor growth curves in b. d) Morbidity-free survival of different groups of MC-38-bearing mice after various treatments. Survival curves are obtained using the Kaplan–Meier method and compared by the log-rank test. e,f) Representative flow cytometry plots (e) and quantifications (f) of $CD8^+$ T cells within the tumor ($n = 4$ biologically independent samples). g,h) Representative flow cytometry plots (g) and quantifications (h) of activated cytotoxic T ($IFN\text{-}\gamma^+CD8^+$) cells within the spleen ($n = 5$ biologically independent samples). i,j) Representative flow cytometry plots (i) and quantifications (j) of $CD4^+$ T cells within the tumor ($n = 5$ biologically independent samples). k) Quantifications of $CD4^+CD25^+FoxP3^+$ regulatory T cells within the tumor ($n = 4$ biologically independent samples). l) Quantifications of effector memory $CD8^+$ T ($CD8^+CD44^+CD62L^-$) cells in peripheral blood mononuclear cells (PBMCs) ($n = 4$ biologically independent samples). m) Quantifications of effector memory $CD4^+$ T ($CD4^+CD44^+CD62L^-$) cells in PBMCs ($n = 3$ biologically independent samples). n,o) IFN-γ spot-forming cells (SFCs) (n) and statistical data (o) from restimulated splenocytes determined by the ELISPOT assay ($n = 4$ biologically independent samples). p) Expression levels of IFN-γ in the serum analyzed by ELISA ($n = 5$ biologically independent samples). q) Expression levels of TNF-α in the serum analyzed by ELISA ($n = 4$ biologically independent samples). Data are presented as mean ± SD and statistical significance was analyzed via one-way ANOVA with Tukey's multiple comparison test. p value: $^*p < 0.05$, $^{**}p < 0.01$, $^{***}p < 0.001$, $^{****}p < 0.0001$.

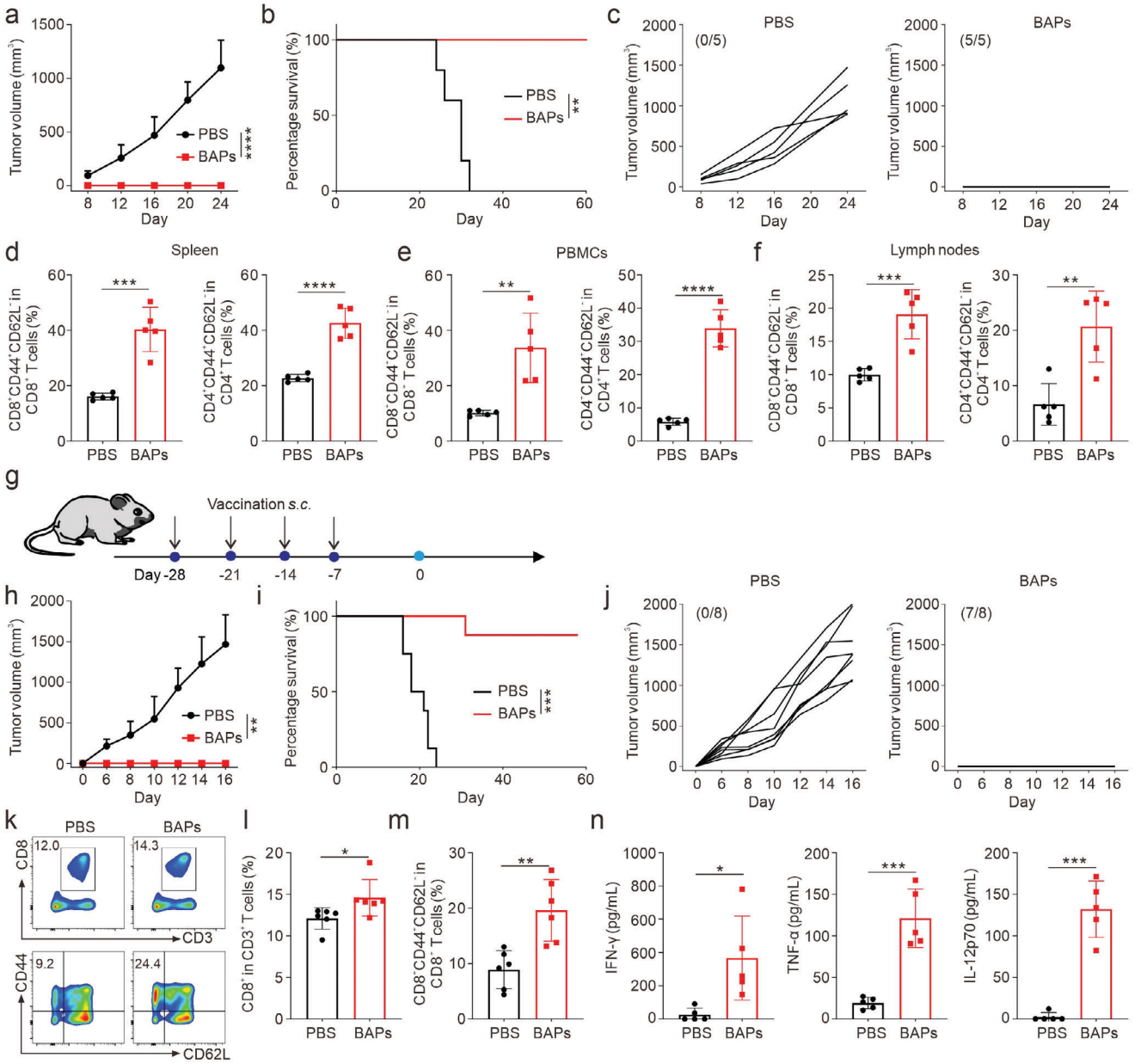

Figure 4. The BAPs nanovaccine protects against tumor rechallenge and prevents tumor occurrence. a) BAPs nanovaccine-immunized mice (complete tumor regression, ≈100 days after primary inoculation) were rechallenged with a subcutaneous flank injection of MC-38 cells, and tumor growth was measured over time (n = 5 biologically independent samples). b) Morbidity-free survival of different groups of MC-38-inoculated mice after various treatments. c) Individual tumor growth curves in a. d–f) Quantifications of effector memory $CD8^+$ and $CD4^+$ T ($CD8^+CD44^+CD62L^-$ and $CD4^+CD44^+CD62L^-$) cells in spleens (d), PBMCs (e), and LN (f) (n = 5 biologically independent samples). g) The timeline of the experimental design to evaluate the preventive performance of BAPs. h) BAPs nanovaccine-immunized mice were inoculated with MC-38 cells, and tumor growth was measured over time (n = 8 biologically independent samples). i) Morbidity-free survival of different groups of MC-38-inoculated mice after various treatments. j) Individual tumor growth curves in h. k–m) Representative flow dot plots (k) and statistical data of $CD8^+$ cytotoxic T cells (l) and effector memory T cells ($CD8^+CD44^+CD62L^-$) (m) in the PBMCs analyzed by flow cytometry (n = 6 biologically independent samples). n) Expression levels of IFN-γ, TNF-α, and IL-12p70 in the serum from mice analyzed by ELISA (n = 5 biologically independent samples). Data are presented as mean ± SD and statistical significance was analyzed via a two-tailed Student's t-test. p value: $^*p < 0.05$, $^{**}p < 0.01$, $^{***}p < 0.001$, $^{****}p < 0.0001$.

tissue resident memory cytotoxic T cells within the spleen was observed in the combination group (Figure 5m). Natural killer (NK) cells play important roles in innate immunity.[21] Treatment with BAPs led to an increase in the fractions of NKG2D-positive NK cells, and this trend was further enhanced following the administration of anti-CTLA4 (Figure 5n). The boosted adaptive and innate immunity was also verified by the up-regulated secretion of cytokines such as TNF-α (Figure 5o). Negligible body weight variation was observed, showing the biosafety of the combinatorial treatment (Figure S13, Supporting Information). These findings

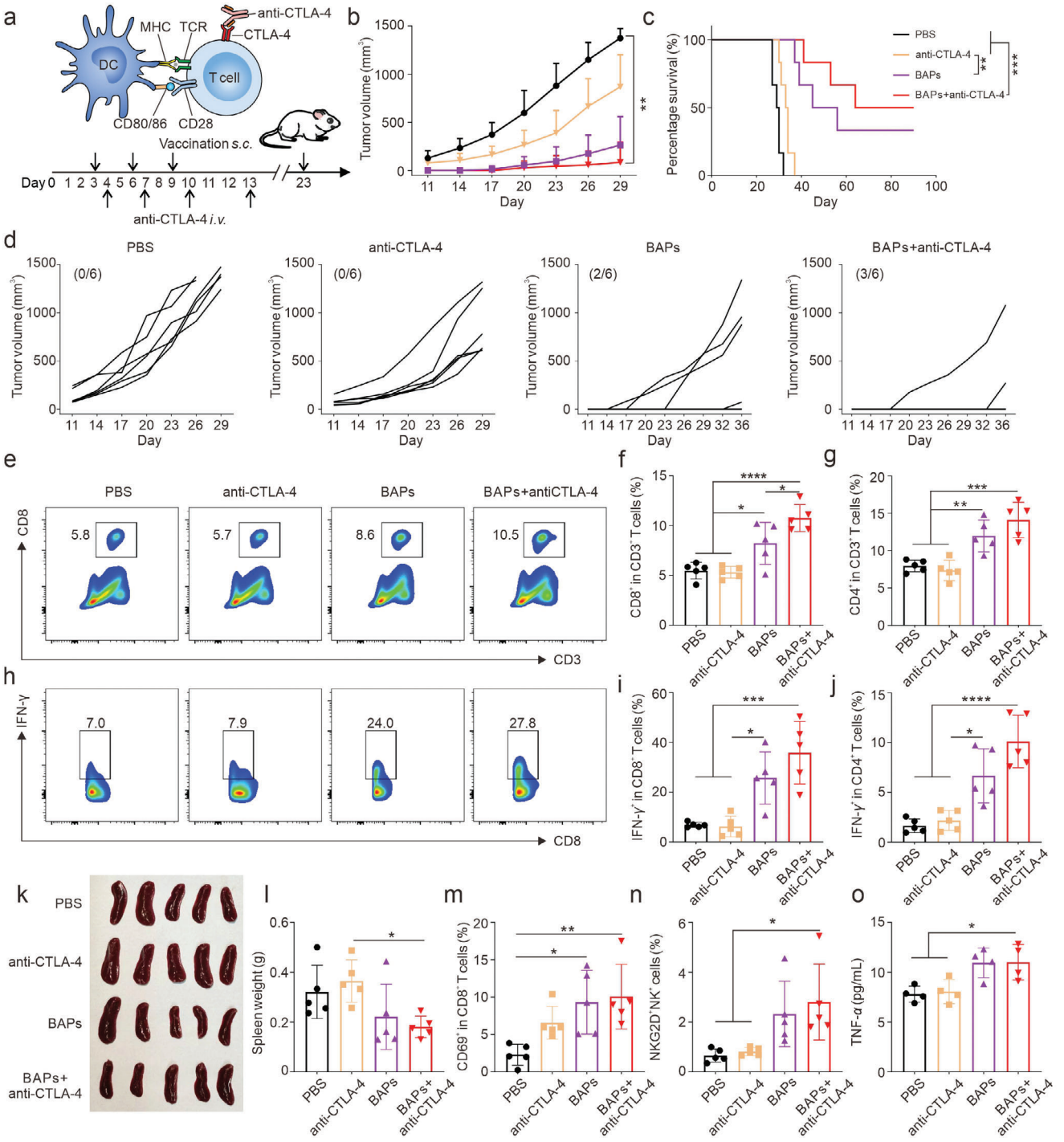

Figure 5. BAPs synergy with ICB therapy to treat 4T1 tumors. a) Schematic illustration of the therapeutic mechanism and timeline of the experimental design. b) Average tumor growth curves of 4T1-bearing mice after various treatments indicated ($n = 6$ biologically independent samples). c) Morbidity-free survival of different groups of 4T1-inoculated mice after various treatments. d) Individual tumor growth curves in b. e,f) Representative flow dot plots (e) and statistical data (f) of $CD8^+$ cytotoxic T cells within the spleen analyzed by flow cytometry. g) Quantification of $CD4^+$ T helper cells within the spleen. h,i) Representative flow dot plots (h) and statistical data of activated IFN-γ^+CD8^+ cytotoxic T cells (i) within the spleen. j) Quantification of activated IFN-γ^+CD4^+ T helper cells within the spleen. k,l) Photographs (k) and corresponding weights (l) of the spleens retrieved from the mice after different treatments. m) Quantification of $CD69^+CD8^+$ tissue resident memory cytotoxic T cells within the spleen. n) Quantification of $NKG2D^+$ NK cells within the spleen. e-n, $n = 5$ biologically independent samples. o) Expression levels of TNF-α in the serum analyzed by ELISA ($n = 4$ biologically independent samples). Data are presented as mean ± SD and statistical significance was analyzed via one-way ANOVA with Tukey's multiple comparison test. p value: $^*p < 0.05$, $^{**}p < 0.01$, $^{***}p < 0.001$, $^{****}p < 0.0001$.

suggest that the synergistic treatment regimen elicited antitumor immune responses, promoted the activation of systematic effector cells, and thereby contributed to overall therapeutic efficacy.

3. Conclusion

In this work, we report a biomimetic approach for producing reinforced biomimetic autophagosome-based personalized nanovaccines. Tumor-specific Ag derived from stimulated TRAPs was integrated with two types of adjuvants, yielding nanosized BAPs nanovaccines that exhibit heightened lymphatic targeting efficacy and enhanced DCs uptake efficiency. Most importantly, Ag derived from TRAPs demonstrated superior immunogenicity compared to commonly shared tumor Ag, including those obtained from whole tumor cells. This resulted in heightened Ag cross-presentation and robust immune responses. The immunogenicity could further be precisely modulated by adjusting the Ag content, presenting an advantage over traditional vaccination methods. In a colon carcinoma model, BAPs demonstrated their potency to generate broad-spectrum T-cell responses, reverse immunosuppression, inhibit tumor growth, and prolong survival in tumor-bearing mice. Furthermore, a strong immune-memory effect was observed, effectively safeguarding the cured mice against tumor rechallenge. By evoking systemic immune responses, BAPs exhibited preventive effects against tumor formation. In particular, the synergistic combination of this enhanced personalized anticancer nanovaccine with ICB therapy has shown considerable promise in the context of personalized cancer immunotherapy, especially for poorly immunogenic tumors. Collectively, this biomimetic strategy represents a valuable avenue for the development of personalized cancer nanovaccines with heightened immunogenicity, with potential implications for clinical translation.

4. Experimental Section

Collection of Tumor Cell-Derived Autophagosomes (TRAPs): When the tumor cells grew to 70%–90% confluence, they were treated with 100 nmol mL^{-1} rapamycin, 100 nmol mL^{-1} bortezomib, and 10 mmol mL^{-1} NH_4Cl in a complete 1640 medium for 24 h. Then the supernatant was collected, and the cells and cell debris were first removed by centrifugation at 2000 rpm, 4 °C, for 10 min. The supernatant was transferred to a new centrifuge tube and centrifuged at 12,000 rpm, 4 °C, for 15 min. The TRAPs were concentrated in the precipitate. The TRAPs were finally resuspended with PBS and stored at −80 °C. Then western blotting was performed according to the standard methods.

Fabrication of Biomimetic Autophagosomes (BAPs) Vaccines: Poly(ethylene glycol)-*b*-poly(trimethylene carbonate-*co*-dithiolane trimethylene carbonate)-spermine (PEG-P(TMC-DTC)-SP) was synthesized according to the previous reports.[14,22] The obtained TRAPs were resuspended in PBS, followed by sonication for at least 6 freeze-thaw cycles. Then, antigens were collected for the preparation of BAPs.

To fabricate BAPs nanovaccines, two adjuvants, the TLR9 agonists CpG and STING agonist ADU-S100 was used, which had theoretical loads of 5.0 wt.% and 2.5 wt.% in the nanovesicles, respectively. Specifically, 100 µL of PEG-P(TMC-DTC)-SP (40 mg mL^{-1} in DMF) was added dropwise to 900 µL of a mixed PBS solution (2 mM, pH 6.0) containing 200 µg of CpG, 100 µg of ADU-S100, and 45 µg of autophagosomal proteins, resulting in the formation of BAPs nanovaccine. Electrostatic interactions facilitated the efficient encapsulation of adjuvants and antigens within the nanovesicles. The resulting solution was stirred for 10 min, followed by a series of gradient dialysis steps: first, in PBS solution (2 mM, pH 6.0) for 2 h; second, in a 1:1 (v/v) mixture of PBS 6.0 and PBS 7.4 for 1 h; and finally, in PBS solution (10 mM, pH 7.4) for 2 h. The drug loading content (DLC) and drug loading efficiency (DLE) of the adjuvants and antigens were quantified using Nanodrop (Thermo Scientific) and the Micro BCA protein assay kit, respectively.

Cell Lines and Animals: MC-38 mouse colorectal cancer cells and 4T1 mouse breast cancer cells were obtained from the Shanghai Institute of Biochemistry and Cell Biology. Cells were maintained in RPMI-1640 medium supplemented with fetal bovine serum (final concentration 10%), 100 U ml^{-1} each of penicillin and streptomycin. All the cells were maintained at 37 °C in a 95% air, 5% CO_2 atmosphere. Female C57BL/6 (6-8 weeks) and BALB/c (6-8 weeks) mice were purchased from Charles River Company (Beijing, China). The in vivo experiments were performed in the context of an animal protocol approved by the Animal Care and Use Committee of Soochow University (202206A0597, 202302A0529).

Phenotypic and Functional Assessment of Immune Cells: For the analysis of the activation of lymphocytes, peripheral blood, tumor tissues, and spleens were harvested from the animals in all the treatment groups at 7 days after the final immunization. For the analysis of tumor cells or tumor-infiltrating T cells, tumor tissues were excised and cut into small pieces of 2–4 mm and then placed in a dissociation buffer (1 mg mL^{-1} collagenase type IV and 0.1 mg mL^{-1} DNase I in RPMI) for 30 min at 37 °C with gentle shaking. For the analysis of lymphocytes in the spleen, single cells were collected by grinding the spleen. All the cells were resuspended in 1× red blood cell lysis buffer (BioLegend) for 10 min to lyse the red blood cells. Then, the cells were passed through a 70 µm strainer, washed with FACS buffer, and stained with CD45-PerCP/Cy5.5, CD3-FITC, CD8-PE, CD107a-Alexa Fluor647, CD4-PE/Cy7, CD25-PE/Cy7, and Foxp3- Alexa Fluor647 accordingly, followed by flow cytometric analysis. The intracellular cytokine staining assays on T cells were performed with anti-IFN-γ-APC.[23] Serum samples were collected 6 h after the final injection to quantify the concentrations of IFN-γ and TNF-α. The main organs (heart, liver, spleen, lung, and kidney) were collected on day 7 post-immunization and maintained in 4% paraformaldehyde. Tissue sections were stained with H&E for histological analysis.

Statistical Analysis: All the experimental data were statistically analyzed, and the results were expressed as a mean ± standard deviation (SD), $n \geq 3$. GraphPad Prism (version number: 8.0) software was used for statistical analysis. Statistical significance was calculated via a two-tailed Student's *t*-test for two-group comparisons. Statistical differences were determined using one-way two-sided analysis of variance (ANOVA) for multiple comparisons. Statistical significance was set as follows: $^{*}p < 0.05$, $^{**}p < 0.01$, $^{***}p < 0.001$, $^{****}p < 0.0001$, and ns denotes no significant difference.

Supporting Information

Supporting Information is available from the Wiley Online Library or from the author.

Acknowledgements

L.Q. and G.C. contributed equally to this work. This work was financially supported by the National Natural Science Foundation of China (52233007), the National Key R&D Program of China (2021YFB3800900), and the Startup Packages of Soochow University (NH13201324).

Conflict of Interest

The authors declare no conflict of interest.

Data Availability Statement

The data that support the findings of this study are available from the corresponding author upon reasonable request.

Keywords

antigen cross-presentation, autophagosome, cancer vaccine, immunotherapy, lymphatic delivery

Received: July 4, 2024
Revised: August 1, 2024
Published online: August 28, 2024

[1] a) F. Lang, B. Schrörs, M. Löwer, Ö. Türeci, U. Sahin, *Nat. Rev. Drug. Discov.* **2022**, *21*, 261; b) D. S. Kuen, J. Hong, S. Lee, C. H. Koh, M. Kwak, B. S. Kim, M. Jung, Y. J. Kim, B. S. Cho, B. S. Kim, *Adv. Mater.* **2023**, *35*, 2303080; c) M. Yarchoan, E. J. Gane, T. U. Marron, R. Perales-Linares, J. Yan, N. Cooch, D. H. Shu, E. J. Fertig, L. T. Kagohara, G. Bartha, J. Northcott, J. Lyle, S. Rochestie, J. Peters, J. T. Connor, E. M. Jaffee, I. Csiki, D. B. Weiner, A. Perales-Puchalt, N. Y. Sardesai, *Nat. Med.* **2024**, *30*, 1044.

[2] a) P. D. Katsikis, K. J. Ishii, C. Schliehe, *Nat. Rev. Immunol.* **2024**, *24*, 213; b) Y. Zheng, Z. Zhong, *J. Controlled Release* **2022**, *347*, 308; c) L. Yang, J. Yang, A. Kleppe, H. E. Danielsen, D. J. Kerr, *Nat. Rev. Clin. Oncol.* **2024**, *21*, 67.

[3] a) E. Blass, P. A. Ott, *Nat. Rev. Clin. Oncol.* **2021**, *18*, 215; b) J. Zhang, B. Fan, G. Cao, W. Huang, F. Jia, G. Nie, H. Wang, *Adv. Mater.* **2022**, *34*, 2205950; c) N. Gong, M.-G. Alameh, R. El-Mayta, L. Xue, D. Weissman, M. J. Mitchell, *Nat. Rev. Drug Discovery* **2024**, *23*, 607.

[4] a) Y. Guo, S.-Z. Wang, X. Zhang, H.-R. Jia, Y.-X. Zhu, X. Zhang, G. Gao, Y.-W. Jiang, C. Li, X. Chen, *Nat. Commun.* **2022**, *13*, 6534; b) Z. Meng, Y. Zhang, X. Zhou, J. Ji, Z. Liu, *Adv. Drug Delivery Rev.* **2022**, *182*, 114107; c) M. J. Lin, J. Svensson-Arvelund, G. S. Lubitz, A. Marabelle, I. Melero, B. D. Brown, J. D. Brody, *Nat. Cancer* **2022**, *3*, 911; d) J. Meng, Y. Lv, W. Bao, Z. Meng, S. Wang, Y. Wu, S. Li, Z. Jiao, Z. Tian, G. Ma, *Nat. Commun.* **2023**, *14*, 4505; e) L. Ma, L. Diao, Z. Peng, Y. Jia, H. Xie, B. Li, J. Ma, M. Zhang, L. Cheng, D. Ding, X. Zhang, H. Chen, F. Mo, H. Jiang, G. Xu, F. Meng, Z. Zhong, *Adv. Mater.* **2021**, *33*, 2104849.

[5] a) L. Diao, M. Liu, *Adv. Sci.* **2023**, *10*, 2300121; b) J. Chen, M. Qiu, Z. Ye, T. Nyalile, Y. Li, Z. Glass, X. Zhao, L. Yang, J. Chen, Q. Xu, *Sci. Adv.* **2021**, *7*, eabf1244; c) L. Fang, Z. Zhao, J. Wang, P. Zhang, Y. Ding, Y. Jiang, D. Wang, Y. Li, *Sci. Adv.* **2020**, *6*, eaba4024.

[6] a) Y. G. Zhao, P. Codogno, H. Zhang, *Nat. Rev. Mol. Cell Biol.* **2021**, *22*, 733; b) J. Debnath, N. Gammoh, K. M. Ryan, *Nat. Rev. Mol. Cell Biol.* **2023**, *24*, 560.

[7] a) Y. Ma, L. Galluzzi, L. Zitvogel, G. Kroemer, *Immunity* **2013**, *39*, 211; b) K. Yamamoto, A. Venida, J. Yano, D. E. Biancur, M. Kakiuchi, S. Gupta, A. S. Sohn, S. Mukhopadhyay, E. Y. Lin, S. Parker, *Nature* **2020**, *581*, 100; c) M. Loi, A. Müller, K. Steinbach, J. Niven, R. B. da Silva, P. Paul, L.-A. Ligeon, A. Caruso, R. A. Albrecht, A. C. Becker, *Cell Rep.* **2016**, *15*, 1076.

[8] a) Y. Li, L.-X. Wang, P. Pang, Z. Cui, S. Aung, D. Haley, B. A. Fox, W. J. Urba, H.-M. Hu, *Clin. Cancer. Res.* **2011**, *17*, 7047; b) R. E. Sanborn, H. J. Ross, S. Aung, A. Acheson, T. Moudgil, S. Puri, T. Hilton, B. Fisher, T. Coffey, C. Paustian, *J. Immunother. Cancer* **2017**, *5*, 103; c) D. B. Page, T. W. Hulett, T. L. Hilton, H.-M. Hu, W. J. Urba, B. A. Fox, *J. Immunother. Cancer* **2016**, *4*, 25; d) T. L. Hilton, T. W. Hulett, C. Dubay, R. van de Ven, S. Aung, W. J. Urba, H. M. Hu, B. A. Fox, *J. Immunother. Cancer* **2013**, *1*, 260; e) H. Ren, T. Zhang, Y. Wang, Q. Yao, Z. Wang, L. Zhang, L. Wang, *Front. Immunol.* **2021**, *12*, 675822.

[9] a) Z.-F. Wen, H. Liu, R. Gao, M. Zhou, J. Ma, Y. Zhang, J. Zhao, Y. Chen, T. Zhang, F. Huang, *J. Immunother. Cancer* **2018**, *6*, 1; b) M. Zhou, Z. Wen, F. Cheng, J. Ma, W. Li, H. Ren, Y. Sheng, H. Dong, L. Lu, H.-M. Hu, L.-X. Wang, *Oncoimmunology* **2016**, *5*, 1180485; c) Y.-Q. Chen, P.-C. Li, N. Pan, R. Gao, Z.-F. Wen, T.-Y. Zhang, F. Huang, F.-Y. Wu, X.-L. Ou, J.-P. Zhang, X.-J. Zhu, H. M. Hu, K. Chen, Y.-L. Cai, L.-X. Wang, *J. Immunother. Cancer* **2019**, *7*, 4509; d) R. Gao, J. Ma, Z. Wen, P. Yang, J. Zhao, M. Xue, Y. Chen, M. Aldarouish, H.-M. Hu, X.-J. Zhu, N. Pan, L.-X. Wang, *Oncoimmunology* **2018**, *7*, 1438108.

[10] a) Y. Li, L.-x. Wang, P. Pang, C. Twitty, B. A. Fox, S. Aung, W. J. Urba, H.-M. Hu, *Autophagy* **2009**, *5*, 576; b) Y. Ding, Z. Li, A. Jaklenec, Q. Hu, *Adv. Drug Delivery Rev.* **2021**, *179*, 113914.

[11] S. Liu, Q. Jiang, X. Zhao, R. Zhao, Y. Wang, Y. Wang, J. Liu, Y. Shang, S. Zhao, T. Wu, *Nat. Mater.* **2021**, *20*, 421.

[12] Y. Li, L.-X. Wang, G. Yang, F. Hao, W. J. Urba, H.-M. Hu, *Cancer Res.* **2008**, *68*, 6889.

[13] C. Liu, X. Liu, X. Xiang, X. Pang, S. Chen, Y. Zhang, E. Ren, L. Zhang, X. Liu, P. Lv, X. Wang, W. Luo, N. Xia, X. Chen, G. Liu, *Nat. Nanotechnol.* **2022**, *17*, 531.

[14] a) Y. Zou, F. Meng, C. Deng, Z. Zhong, *J. Controlled Release* **2016**, *239*, 149; b) W. Gu, J. An, H. Meng, N. Yu, Y. Zhong, F. Meng, Y. Xu, J. J. Cornelissen, Z. Zhong, *Adv. Mater.* **2019**, *31*, 1904742; c) J. Wang, B. Guo, Z. Sun, S. Zhao, L. Cao, Z. Zhong, F. Meng, *Adv. Healthcare Mater.* **2024**, 2400784, https://doi.org/10.1002/adhm.202400784.

[15] a) Y. Li, X. Li, J. Yi, Y. Cao, Z. Qin, Z. Zhong, W. Yang, *Adv. Healthcare Mater.* **2023**, *12*, 2300260; b) H. Zheng, B. Guo, X. Qiu, Y. Xia, Y. Qu, L. Cheng, F. Meng, Z. Zhong, *Bioact. Mater.* **2022**, *16*, 1.

[16] M. Gouez, A. Rébillard, A. Thomas, S. Beaumel, E.-L. Matera, E. Gouraud, L. Orfila, B. Martin, O. Pérol, C. Chaveroux, *Front. Immunol.* **2024**, *15*, 1368550.

[17] a) K. Das, E. Belnoue, M. Rossi, T. Hofer, S. Danklmaier, T. Nolden, L.-M. Schreiber, K. Angerer, J. Kimpel, S. Hoegler, *Nat. Commun.* **2021**, *12*, 5195; b) Y. Yue, J. Xu, Y. Li, K. Cheng, Q. Feng, X. Ma, N. Ma, T. Zhang, X. Wang, X. Zhao, G. Nie, *Nat. Biomed. Eng.* **2022**, *6*, 898; c) M. Tang, B. Chen, H. Xia, M. Pan, R. Zhao, J. Zhou, Q. Yin, F. Wan, Y. Yan, C. Fu, L. Zhong, Q. Zhang, Y. Wang, *Nat. Commun.* **2023**, *14*, 5888; d) Z. Wang, T. You, Q. Su, W. Deng, J. Li, S. Hu, S. Shi, Z. Zou, J. Xiao, X. Duan, *Adv. Mater.* **2023**, *35*, 2307193.

[18] E. Salvatori, L. Lione, M. Compagnone, E. Pinto, A. Conforti, G. Ciliberto, L. Aurisicchio, F. Palombo, *npj Vaccines* **2022**, *7*, 15.

[19] Y. Huang, Z. Guan, X. Dai, Y. Shen, Q. Wei, L. Ren, J. Jiang, Z. Xiao, Y. Jiang, D. Liu, *Nat. Commun.* **2021**, *12*, 4310.

[20] a) J. Xu, J. Lv, Q. Zhuang, Z. Yang, Z. Cao, L. Xu, P. Pei, C. Wang, H. Wu, Z. Dong, Y. Chao, C. Wang, K. Yang, R. Peng, Y. Cheng, Z. Liu, *Nat. Nanotechnol.* **2020**, *15*, 1043; b) Y. C. Zeng, O. J. Young, C. M. Wintersinger, F. M. Anastassacos, J. I. MacDonald, G. Isinelli, M. O. Dellacherie, M. Sobral, H. Bai, A. Graveline, A. Vernet, M. Sanchez, K. Mulligan, Y. Choi, T. C. Ferrante, D. B. Keskin, G. G. Fell, D. Neuberg, C. J. Wu, D. Mooney, I. C. Kwon, J. H. Ryu, W. M. Shih, *Nat. Nanotechnol.* **2024**, *19*, 1055; c) D. Ji, Y. Zhang, J. Sun, B. Zhang, W. Ma, B. Cheng, X. Wang, Y. Li, Y. Mu, H. Xu, Q. Wang, C. Zhang, S. Xiao, L. Zhang, D. Zhou, *Nat. Biotechnol.* **2024**, *42*, 518; d) I. Mota, E. Patrucco, C. Mastini, N. R. Mahadevan, T. C. Thai, E. Bergaggio, T.-C. Cheong, G. Leonardi, E. Karaca-Atabay, M. Campisi, *Nat. Cancer* **2023**, *4*, 1016; e) Y. Chao, C. Liang, H. Tao, Y. Du, D. Wu, Z. Dong, Q. Jin, G. Chen, J. Xu, Z. Xiao, Q. Chen, C. Wang, J. Chen, Z. Liu, *Sci. Adv.* **2020**, *6*, eaaz4204.

[21] N. K. Wolf, D. U. Kissiov, D. H. Raulet, *Nat. Rev. Immunol.* **2023**, *23*, 90.

[22] a) G. Cui, Y. Sun, L. Qu, C. Shen, Y. Sun, F. Meng, Y. Zheng, Z. Zhong, *Adv. Healthcare Mater.* **2024**, 2303690; b) X. Qiu, Y. Qu, B. Guo, H. Zheng, F. Meng, Z. Zhong, *J. Controlled Release* **2022**, *341*, 498; c) W. Gu, T. Liu, D. Fan, J. Zhang, Y. Xia, F. Meng, Y. Xu, J. J. Cornelissen, Z. Liu, Z. Zhong, *J. Controlled Release* **2021**, *329*, 706; d) Y. Zhang, S. Yue, R. Haag, H. Sun, Z. Zhong, *J. Controlled Release* **2021**, *340*, 331.

[23] a) S. Wang, Y. Zhang, Y. Wang, Y. Yang, S. Zhao, T. Sheng, Y. Zhang, Z. Gu, J. Wang, J. Yu, *Nat. Commun.* **2023**, *14*, 6953; b) Y. Zhang, S. Wang, Y. Yang, S. Zhao, J. You, J. Wang, J. Cai, H. Wang, J. Wang, W. Zhang, *Nat. Commun.* **2023**, *14*, 3431.